Appl. Math. Mech. -Engl. Ed., **42**(11), 1599–1618 (2021)

APPLIED MATHEMATICS AND MECHANICS (ENGLISH EDITION)

https://doi.org/10.1007/s10483-021-2783-9

Static response of functionally graded multilayered two-dimensional quasicrystal plates with mixed boundary conditions*

Xin FENG[1], Liangliang ZHANG[2], Yuxuan WANG[2],
Jinming ZHANG[2], Han ZHANG[3], Yang GAO[2,†]

1. College of Engineering, China Agricultural University, Beijing 100083, China;
2. College of Science, China Agricultural University, Beijing 100083, China;
3. China State Key Laboratory of Acoustics, Institute of Acoustics,
Chinese Academy of Sciences, Beijing 100190, China

(Received Jul. 14, 2021 / Revised Sept. 2, 2021)

Abstract The unusual properties of quasicrystals (QCs) have attracted tremendous attention from researchers. In this paper, a semi-analytical solution is presented for the static response of a functionally graded (FG) multilayered two-dimensional (2D) decagonal QC rectangular plate with mixed boundary conditions. Based on the elastic theory of FG 2D QCs, the state-space method is used to derive the state equations composed of partial differential along the thickness direction. Besides, the Fourier series expansion and the differential quadrature technique are utilized to simulate the simply supported boundary conditions and the mixed boundary conditions, respectively. Then, the propagator matrix which connects the field variables at the upper interface to those at the lower interface of any homogeneous layer can be derived based on the state equations. Combined with the interface continuity condition, the static response can be obtained by imposing the sinusoidal load on the top surfaces of laminates. Finally, the numerical examples are presented to verify the effectiveness of this method, and the results are very useful for the design and understanding of the characterization of FG QC materials in their applications to multilayered systems.

Key words two-dimensional (2D) quasicrystal (QC) laminate, functionally graded material (FGM), mixed boundary condition, static response, differential quadrature technique

Chinese Library Classification O343.8
2010 Mathematics Subject Classification 52C23, 74K20, 74B99

* Citation: FENG, X., ZHANG, L. L., WANG, Y. X., ZHANG, J. M., ZHANG, H., and GAO, Y. Static response of functionally graded multilayered two-dimensional quasicrystal plates with mixed boundary conditions. *Applied Mathematics and Mechanics* (*English Edition*), **42**(11), 1599–1618 (2021) https://doi.org/10.1007/s10483-021-2783-9

† Corresponding author, E-mail: gaoyangg@gmail.com

Project supported by the National Natural Science Foundation of China (Nos. 11972354, 11972365, and 12102458) and the China Agricultural University Education Foundation (No. 1101-2412001)

1 Introduction

Quasicrystals (QCs), which possess the long-range quasi-periodic translational order and the long-range orientational order, were first discovered by Shechtman et al.[1]. Due to their unique quasi-periodic structure, QCs have many excellent properties, such as high hardness, high toughness, high abrasion resistance, high resistivity, low friction coefficient, and low thermal conductivity[2–4]. These attractive properties of QCs enable them to have many potential applications, such as solar thin film, thermoelectric converter, and structural enhancement phase of composites[5–8]. In particular, when QC thin film was used for solar panels, the mismatch of the material coefficients between the thin film and substrate materials may initiate debonding and micro-cracks[9–10]. Thus, functionally gradient materials (FGMs) can be introduced to overcome these defects[11].

Moreover, FGMs can also be utilized to surmount the delamination and cracking problems of multilayered composite structure models. Due to their special structural features, FGMs have attracted attention from scientists. Based on the modified couple-stress theory, Guo et al.[12–13] presented the three-dimensional (3D) size-dependent multilayered model for simply supported and functionally graded (FG) anisotropic elastic composite plates. According to the two-dimensional (2D) higher-order deformation theory, Matsunaga[14] derived the solution of free vibration and stability for FG shallow shells. By virtue of the state-space method, Huang et al.[15] derived the benchmark solutions for FG thick plates resting on the two-parameter foundation model. After that, Lu et al.[16] presented the free vibration analysis of FG thick plates on an elastic foundation by using the same method. Based on 3D thermoelasticity, Ying et al.[17] investigated the thermal-mechanical behavior of FG thick plates.

Meanwhile, researchers have also studied the mechanical properties of FG QC materials. Based on the linear elastic theory of QCs , Huang et al.[18] presented a mechanical model of FG one-dimensional (1D) hexagonal piezoelectric QC laminates by using the state vector method, and investigated the influence of FG exponential factor on the static response of the laminates. Zhang et al.[19] derived the static bending deformation of FGM 1D hexagonal piezoelectric QC laminates with a nonlocal effect. Li et al.[20] obtained the exact solution for the FG multilayered 1D orthorhombic QC plate. By virtue of the pseudo-Stroh method and the propagator matrix method, Li et al.[21] investigated the thermo-elastic solution of FG multilayered 2D decagonal QC plates with simply supported boundary conditions. Furthermore, Li et al.[22] obtained the exact solution of FGM 2D piezoelectric QC laminate by using the same methods. Other numerous studies on the dynamic behaviors of QC plates such as free vibration[23] and harmonic response[24] of FG QC laminates have been performed. However, in the studies mentioned above, the FG QC laminates were analyzed with simply supported boundary conditions. Although the pseudo-Stroh formalism[10,12,20–21] and the state-space method[15–18] have been used to derive the FG plates with simply supported boundary conditions according to the general solutions of the extended displacements and stresses, the plates with clamped-supported and mixed boundary conditions cannot be solved.

Some semi-analytical numerical methods[25–27] can be used to derive the solutions of the static response and free vibration for plates with arbitrary boundary conditions. However, the differential quadrature method (DQM) has been approved to be highly efficient for the rapid solution of differential equations governing boundary/initial problems during the past decades[28–29]. In addition, it is convenient for this method to deal with arbitrary supporting conditions and reduce the dimension of the final governing equations. The DQM is a numerical method that can be used to solve ordinary differential, partial differential, integral, and integrodifferential equations[30]. It has potential application prospects in various typical boundary value and initial value problems. Wang[28] collected more than sixty related documents to summarize the application status of the DQM in the field of structural mechanics, and pointed out the urgent problems to be manipulated. By using the DQM, Lu et al.[27] analyzed the free

vibration of laminated plates under mixed boundary conditions. Under the arbitrary boundary conditions, Zhou et al.[29,31] used the same method to analyze the dynamic response of piezoelectric plates and the cylindrical bending with imperfect interfaces for piezoelectric laminates. Yas et al.[32] and Yas and Moloudi[33] presented the solution of the free vibration for a piezoelectric ring plate with changes exponentially along the thickness direction, and studied the influence of the Winkler elastic foundation constant on the natural frequency of the plate under different boundary conditions.

In this paper, the state-space based differential quadrature method (SS-DQM) is developed to investigate the static response problems for FG 2D QC thick plates with mixed boundary conditions. We extend the state-space method to the FG 2D QC material with multiple physical coupling fields, from which the basic elasticity equation is converted to a linear control system. Compared with the general solution of the extended displacements and stresses for the four-side simple supported QC plate[20–21], the Fourier series expansion and the differential quadrature technique are effective methods to satisfy the simply supported boundary conditions and the mixed boundary conditions. The propagator matrix method is used to obtain the semi-analytical solution of the FG 2D QC laminates. Finally, numerical examples are presented to verify the accuracy of the SS-DQM and illustrate the influence of different boundary conditions, stacking sequences, and FG exponential factors on the phonon and phason variables. The numerical results indicate that the hybrid method is an effective tool to predict the accurate behavior of FG QC composite laminated structures with mixed boundary conditions. Meanwhile, the numerical results can also serve as a reference for verifying existing or future FG QC plate theories.

2 Basic formulations

Consider an M-layer FG 2D QC rectangular plate with the total thickness H in the vertical direction and horizontal dimensions $x\times y = L_x\times L_y$, as shown in Fig. 1. The atomic arrangement of the 2D decagonal QC is quasi-periodic in the xy-plane and periodic along the z-direction. The relationship between the global Cartesian coordinate system and the local material coordinate system of the plates is assumed to be $(x, y, z) = (x_1, x_2, x_3)$. The pth-layer with the thickness $h_p = z_p - z_{p-1}$ $(p = 0, 1, 2, 3, \cdots, M)$ is defined as p in the multilayer plate. It follows that the bottom and top surfaces of the laminate are $z_0 = 0$ and $z_M = H$, respectively. Each layer is defined as homogeneous or FG with exponentially varying material properties.

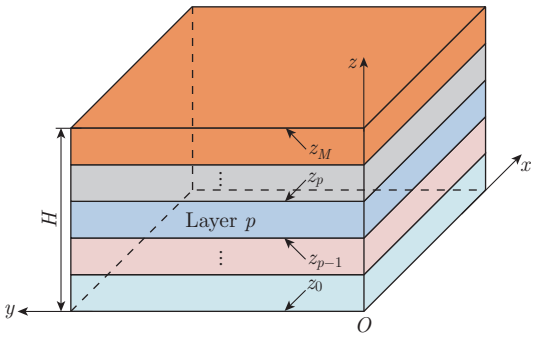

Fig. 1 An M-layered FG 2D QC laminate (color online)

2.1 Basic equations

According to the linear elastic theory of QCs[34–36], the generalized relationship of strain-

displacement for 2D QCs are

$$\varepsilon_{ij} = (u_{i,j} + u_{j,i})/2, \quad w_{\alpha j} = w_{\alpha,j}, \tag{1}$$

where i, $j = 1, 2, 3$, and $\alpha = 1, 2$. ε_{ij} and $w_{\alpha j}$ represent the strains in the phonon and phason fields, respectively, u_i and w_α are the phonon and phason displacements, respectively, and the subscript comma denotes partial differentiation with respect to the axis.

The static equilibrium equations without the body force can be written as[37–40]

$$\sigma_{ij,j} = 0, \quad H_{\alpha j,j} = 0, \tag{2}$$

where σ_{ij} denote the phonon stresses, and $H_{\alpha j}$ are the phason stresses.

The stress-strain relationship for 2D decagonal QCs with point groups $10mm$, 1022, $\overline{10}m2$, and $10/mmm$ can be expressed as[41–43]

$$\begin{cases} \sigma_{11} = C_{11}\varepsilon_{11} + C_{12}\varepsilon_{22} + C_{13}\varepsilon_{33} + R_1(w_{11} + w_{22}), \\ \sigma_{22} = C_{12}\varepsilon_{11} + C_{11}\varepsilon_{22} + C_{13}\varepsilon_{33} - R_1(w_{11} + w_{22}), \\ \sigma_{33} = C_{13}\varepsilon_{11} + C_{13}\varepsilon_{22} + C_{33}\varepsilon_{33}, \quad \sigma_{23} = \sigma_{32} = 2C_{44}\varepsilon_{23}, \\ \sigma_{31} = \sigma_{13} = 2C_{44}\varepsilon_{13}, \quad \sigma_{12} = \sigma_{21} = 2C_{66}\varepsilon_{12} - R_1 w_{12} + R_1 w_{21}, \\ H_{11} = R_1(\varepsilon_{11} - \varepsilon_{22}) + K_1 w_{11} + K_2 w_{22}, \\ H_{22} = R_1(\varepsilon_{11} - \varepsilon_{22}) + K_1 w_{22} + K_2 w_{11}, \\ H_{23} = K_4 w_{23}, \quad H_{12} = -2R_1\varepsilon_{12} + K_1 w_{12} - K_2 w_{21}, \\ H_{13} = K_4 w_{13}, \quad H_{21} = 2R_1\varepsilon_{12} - K_2 w_{12} + K_1 w_{21}, \end{cases} \tag{3}$$

where C_{11}, C_{12}, C_{13}, C_{33}, and C_{44} are the elastic constants with the relationship $2C_{66} = C_{11} - C_{12}$ in the phonon field, and K_l $(l = 1, 2, 4)$ and R_1 represent the phason elastic constants and the phonon-phason coupling elastic constant, respectively.

It is assumed that the material properties of the FG QC are exponentially distributed along the z-direction. Therefore, the material constants in Eq. (3) can be rewritten as

$$F(z) = F^0 \mathrm{e}^{\eta z}, \tag{4}$$

where η is the exponential factor characterizing the degree of the material gradient in the z-direction, and F^0 indicates the initial values of the material constants in Eq. (3). It follows that $\eta = 0$ represents the homogeneous QC material case.

2.2 Formulation of state-space method

Substituting Eqs. (1) and (3) into Eq. (2), and according to the state-space method for the QC plate[18], we derive the state equations in matrix forms as

$$\frac{\partial}{\partial z}\boldsymbol{\theta} = \boldsymbol{D}\boldsymbol{\theta}, \tag{5}$$

where $\boldsymbol{\theta} = [u_x, u_y, w_x, w_y, \sigma_{zz}, \sigma_{xz}, \sigma_{yz}, H_{xz}, H_{yz}, u_z]^{\mathrm{T}}$ is called the basic variable matrix, in which the superscript 'T' denotes transpose, and the state transition matrix $\boldsymbol{D}$ is

$$\boldsymbol{D} = \begin{pmatrix} \boldsymbol{0} & \boldsymbol{D}_1 \\ \boldsymbol{D}_2 & \boldsymbol{0} \end{pmatrix}. \tag{6}$$

The submatrices $\boldsymbol{D}_1$ and $\boldsymbol{D}_2$ in Eq. (6) are

$$\boldsymbol{D}_1 = \begin{pmatrix} a_2 & & & & \\ 0 & a_2 & & & \text{Sym.} \\ 0 & 0 & b_3 & & \\ 0 & 0 & 0 & b_3 & \\ -\dfrac{\partial}{\partial x} & -\dfrac{\partial}{\partial y} & 0 & 0 & 0 \end{pmatrix},$$

$$\boldsymbol{D}_2=\begin{pmatrix} -a_1\dfrac{\partial^2}{\partial x^2}-a_6\dfrac{\partial^2}{\partial y^2} & & & & \\ -(a_3+a_6)\dfrac{\partial^2}{\partial x\partial y} & -a_6\dfrac{\partial^2}{\partial x^2}-a_1\dfrac{\partial^2}{\partial y^2} & & & \text{Sym.} \\ -b_1\dfrac{\partial^2}{\partial x^2}+b_1\dfrac{\partial^2}{\partial y^2} & 2b_1\dfrac{\partial^2}{\partial x\partial y} & -b_2\dfrac{\partial^2}{\partial x^2}-b_2\dfrac{\partial^2}{\partial y^2} & & \\ -2b_1\dfrac{\partial^2}{\partial x\partial y} & -b_1\dfrac{\partial^2}{\partial x^2}+b_1\dfrac{\partial^2}{\partial y^2} & 0 & -b_2\dfrac{\partial^2}{\partial x^2}-b_2\dfrac{\partial^2}{\partial y^2} & \\ a_4\dfrac{\partial}{\partial x} & a_4\dfrac{\partial}{\partial y} & 0 & 0 & a_5 \end{pmatrix}, \quad (7)$$

where Sym. denotes a symmetric matrix. The coefficients in Eq. (7) and the following equations can be found in Appendix A.

The remaining stress components in the plate can be expressed as

$$\begin{cases} \sigma_{xx}=a_1\dfrac{\partial u_x}{\partial x}+a_3\dfrac{\partial u_y}{\partial y}+b_1\dfrac{\partial w_x}{\partial x}+b_1\dfrac{\partial w_y}{\partial y}-a_4\sigma_{zz}, \\ \sigma_{yy}=a_3\dfrac{\partial u_x}{\partial x}+a_1\dfrac{\partial u_y}{\partial y}-b_1\dfrac{\partial w_x}{\partial x}-b_1\dfrac{\partial w_y}{\partial y}-a_4\sigma_{zz}, \\ \sigma_{xy}=a_6\dfrac{\partial u_x}{\partial y}+a_6\dfrac{\partial u_y}{\partial x}-b_1\dfrac{\partial w_x}{\partial y}+b_1\dfrac{\partial w_y}{\partial x}, \\ H_{xx}=b_1\dfrac{\partial u_x}{\partial x}-b_1\dfrac{\partial u_y}{\partial y}+b_2\dfrac{\partial w_x}{\partial y}+b_4\dfrac{\partial w_y}{\partial y}, \\ H_{yy}=b_1\dfrac{\partial u_x}{\partial x}-b_1\dfrac{\partial u_y}{\partial y}+b_4\dfrac{\partial w_x}{\partial x}+b_2\dfrac{\partial w_y}{\partial y}, \\ H_{xy}=-b_1\dfrac{\partial u_x}{\partial y}-b_1\dfrac{\partial u_y}{\partial x}+b_2\dfrac{\partial w_x}{\partial y}-b_4\dfrac{\partial w_y}{\partial x}, \\ H_{yx}=b_1\dfrac{\partial u_x}{\partial y}+b_1\dfrac{\partial u_y}{\partial x}-b_4\dfrac{\partial w_x}{\partial y}+b_2\dfrac{\partial w_y}{\partial x}. \end{cases} \quad (8)$$

Consider the simply supported boundary conditions of the FG 2D QC laminate in the y-direction,

$$L_y:\ u_x=u_z=w_x=\sigma_{yy}=H_{yy}=0 \quad \text{at} \quad y=0. \quad (9)$$

We assume that the general solutions[31,44] of laminate are

$$\begin{pmatrix} u_x(x,y,z) \\ u_y(x,y,z) \\ w_x(x,y,z) \\ w_y(x,y,z) \\ \sigma_{zz}(x,y,z) \\ \sigma_{xz}(x,y,z) \\ \sigma_{yz}(x,y,z) \\ H_{xz}(x,y,z) \\ H_{yz}(x,y,z) \\ u_z(x,y,z) \end{pmatrix}=\sum_{n=1}^{\infty}\begin{pmatrix} \widetilde{u}_x(x,z)\sin(qy) \\ \widetilde{u}_y(x,z)\cos(qy) \\ \widetilde{w}_x(x,z)\sin(qy) \\ \widetilde{w}_y(x,z)\cos(qy) \\ \widetilde{\sigma}_{zz}(x,z)\sin(qy) \\ \widetilde{\sigma}_{xz}(x,z)\sin(qy) \\ \widetilde{\sigma}_{yz}(x,z)\cos(qy) \\ \widetilde{H}_{xz}(x,z)\sin(qy) \\ \widetilde{H}_{yz}(x,z)\cos(qy) \\ \widetilde{u}_z(x,z)\sin(qy) \end{pmatrix}, \quad (10)$$

where $q = n\pi/L_y$, n is the number of superposition, and $\widetilde{u}_x, \widetilde{u}_y, \widetilde{w}_x, \widetilde{w}_y, \widetilde{\sigma}_{zz}, \widetilde{\sigma}_{xz}, \widetilde{\sigma}_{yz}, \widetilde{H}_{xz}, \widetilde{H}_{yz}$, and $\widetilde{u}_z$ are unknown functions.

Incorporating Eq. (5) with Eq. (10) yields

$$\frac{\partial}{\partial z}\widetilde{\boldsymbol{\theta}} = \widetilde{\boldsymbol{D}}\widetilde{\boldsymbol{\theta}}, \tag{11}$$

where $\widetilde{\boldsymbol{\theta}}(x,z) = (\widetilde{u}_x, \widetilde{u}_y, \widetilde{w}_x, \widetilde{w}_y, \widetilde{\sigma}_{zz}, \widetilde{\sigma}_{xz}, \widetilde{\sigma}_{yz}, \widetilde{H}_{xz}, \widetilde{H}_{yz}, \widetilde{u}_z)^{\mathrm{T}}$, and $\widetilde{\boldsymbol{D}}$ is the coefficient matrix.

Substituting Eq. (10) into Eq. (8), the equations can be rewritten as

$$\begin{cases} \widetilde{\sigma}_{xx} = a_1\dfrac{\partial \widetilde{u}_x}{\partial x} - a_3 q\widetilde{u}_y + b_1\dfrac{\partial \widetilde{w}_x}{\partial x} - b_1 q\widetilde{w}_y - a_4\widetilde{\sigma}_{zz}, \\ \widetilde{\sigma}_{yy} = a_3\dfrac{\partial \widetilde{u}_x}{\partial x} - a_1 q\widetilde{u}_y - b_1\dfrac{\partial \widetilde{w}_x}{\partial x} + b_1 q\widetilde{w}_y - a_4\widetilde{\sigma}_{zz}, \\ \widetilde{\sigma}_{xy} = a_6 q\widetilde{u}_x + a_6\dfrac{\partial \widetilde{u}_y}{\partial x} - b_1 q\widetilde{w}_x + b_1\dfrac{\partial \widetilde{w}_y}{\partial x}, \\ \widetilde{H}_{xx} = b_1\dfrac{\partial \widetilde{u}_x}{\partial x} + b_1 q\widetilde{u}_y + b_2\dfrac{\partial \widetilde{w}_x}{\partial x} - b_4 q\widetilde{w}_y, \\ \widetilde{H}_{yy} = b_1\dfrac{\partial \widetilde{u}_x}{\partial x} + b_1 q\widetilde{u}_y + b_4\dfrac{\partial \widetilde{w}_x}{\partial x} - b_2 q\widetilde{w}_y, \\ \widetilde{H}_{xy} = -b_1 q\widetilde{u}_x - b_1\dfrac{\partial \widetilde{u}_y}{\partial x} + b_2 q\widetilde{w}_x - b_4\dfrac{\partial \widetilde{w}_y}{\partial x}, \\ \widetilde{H}_{yx} = b_1 q\widetilde{u}_x + b_1\dfrac{\partial \widetilde{u}_y}{\partial x} - b_4 q\widetilde{w}_x + b_2\dfrac{\partial \widetilde{w}_y}{\partial x}. \end{cases} \tag{12}$$

2.3 Formulations of SS-DQM

For a QC laminate with boundary conditions in the x-direction other than the simply supported conditions in Eq. (9), it is difficult to obtain the general solutions satisfying these boundary conditions. However, the SS-DQM can be utilized to overcome the difficulty. Theoretically, the discrete pattern in the x-direction can be divided into five kinds. However, the distribution of grid points has a direct effect on the convergence and computational stability of the algorithm in the differential quadrature technique. This paper adopts the Chebyshev-Gauss-Lobatto grid space model in the in-plane discrete direction[45–46],

$$x_r = \frac{L_x}{2}\Big(1 - \cos\Big(\frac{r-1}{N-1}\pi\Big)\Big), \quad r = 1, 2, 3, \cdots, N, \tag{13}$$

where N is the number of sampling points.

Consider the following two typical supporting conditions[47] at $x = 0$ and $x = L_x$:

$$\text{Simply supported (S): } \widetilde{u}_{yd} = \widetilde{u}_{zd} = \widetilde{w}_{yd} = \widetilde{\sigma}_{xxd} = \widetilde{H}_{xxd} = 0, \tag{14}$$

$$\text{Clamped supported (C): } \widetilde{u}_{xd} = \widetilde{u}_{yd} = \widetilde{u}_{zd} = \widetilde{w}_{xd} = \widetilde{w}_{yd} = 0, \tag{15}$$

where $d = 1$ or N; 'S' indicates the simply supported boundary condition, and 'C' is the clamped supported boundary condition. For example, 'CSCS' denotes a plate with the clamped supported boundary condition at $x = 0$ and $x = L_x$, and the simply supported conditiion at $y = 0$ and $y = L_y$.

Applying the rules in Eqs. (11) and (13), the variables in Eq. (11) are discretized in the x-direction, and the ordinary differential equation at the arbitrary discrete point can be rewritten

as follows:

$$
\begin{cases}
\dfrac{\mathrm{d}\widetilde{u}_{xr}}{\mathrm{d}z} = a_2\widetilde{\sigma}_{xzr} - \displaystyle\sum_{k=1}^{N} X_{rk}^{(1)}\widetilde{u}_{zk}, \quad \dfrac{\mathrm{d}\widetilde{u}_{yr}}{\mathrm{d}z} = a_2\widetilde{\sigma}_{yzr} - q\widetilde{u}_{zr}, \\
\dfrac{\mathrm{d}\widetilde{w}_{xr}}{\mathrm{d}z} = b_3\widetilde{H}_{xzr}, \quad \dfrac{\mathrm{d}\widetilde{w}_{yr}}{\mathrm{d}z} = b_3\widetilde{H}_{yzr}, \quad \dfrac{\mathrm{d}\widetilde{\sigma}_{zzr}}{\mathrm{d}z} = -\displaystyle\sum_{k=1}^{N} X_{rk}^{(1)}\widetilde{\sigma}_{xzr} + q\widetilde{\sigma}_{yzr}, \\
\dfrac{\mathrm{d}\widetilde{\sigma}_{xzr}}{\mathrm{d}z} = -a_1\displaystyle\sum_{k=1}^{N} X_{rk}^{(2)}\widetilde{u}_{xk} + a_6q^2\widetilde{u}_{xr} + (a_3+a_6)q\sum_{k=1}^{N} X_{rk}^{(1)}\widetilde{u}_{yk} - b_1\sum_{k=1}^{N} X_{rk}^{(2)}\widetilde{w}_{xk} \\
\qquad\qquad - b_1q^2\widetilde{w}_{xr} + 2b_1q\displaystyle\sum_{k=1}^{N} X_{rk}^{(1)}\widetilde{w}_{yk} + a_4\sum_{k=1}^{N} X_{rk}^{(1)}\widetilde{\sigma}_{zzk}, \\
\dfrac{\mathrm{d}\widetilde{\sigma}_{yzr}}{\mathrm{d}z} = -(a_3+a_6)q\displaystyle\sum_{k=1}^{N} X_{rk}^{(1)}\widetilde{u}_{xk} - a_6\sum_{k=1}^{N} X_{rk}^{(2)}\widetilde{u}_{yk} + a_1q^2\widetilde{u}_{yr} \\
\qquad\qquad + 2b_1q\displaystyle\sum_{k=1}^{N} X_{rk}^{(1)}\widetilde{w}_{xk} - b_1\sum_{k=1}^{N} X_{rk}^{(2)}\widetilde{w}_{yk} - b_1q^2\widetilde{w}_{yr} + a_4q\widetilde{\sigma}_{zzr}, \\
\dfrac{\mathrm{d}\widetilde{H}_{xzr}}{\mathrm{d}z} = -b_1\displaystyle\sum_{k=1}^{N} X_{rk}^{(2)}\widetilde{u}_{xk} - b_1q^2\widetilde{u}_{xr} - 2b_1q\sum_{k=1}^{N} X_{rk}^{(1)}\widetilde{u}_{yk} - b_2\sum_{k=1}^{N} X_{rk}^{(2)}\widetilde{w}_{xk} + b_2q^2\widetilde{w}_{xr}, \\
\dfrac{\mathrm{d}\widetilde{H}_{yzr}}{\mathrm{d}z} = -2b_1q\displaystyle\sum_{k=1}^{N} X_{rk}^{(1)}\widetilde{u}_{xk} - b_1\sum_{k=1}^{N} X_{rk}^{(2)}\widetilde{u}_{yj} - b_1q^2\widetilde{u}_{yr} - b_2\sum_{k=1}^{N} X_{rk}^{(2)}\widetilde{w}_{yk} + b_2q^2\widetilde{w}_{yr}, \\
\dfrac{\mathrm{d}\widetilde{u}_{zr}}{\mathrm{d}z} = a_4\displaystyle\sum_{k=1}^{N} X_{rk}^{(1)}\widetilde{u}_{xk} - a_4q\widetilde{u}_{yr} + a_5\widetilde{\sigma}_{zzr},
\end{cases}
\tag{16}
$$

where $X_{rk}^{(m)}$ $(1 \leqslant m \leqslant N-1)$ are the differential quadrature weight coefficients.

Similarly, at the same discrete point, Eq. (12) can be rewritten as

$$
\begin{cases}
\widetilde{\sigma}_{xxr} = a_1\displaystyle\sum_{k=1}^{N} X_{rk}^{(1)}\widetilde{u}_{xk} - a_3q\widetilde{u}_{yr} + b_1\sum_{k=1}^{N} X_{rk}^{(1)}\widetilde{w}_{xk} - b_1q\widetilde{w}_{yr} - a_4\widetilde{\sigma}_{zzr}, \\
\widetilde{\sigma}_{yyr} = a_3\displaystyle\sum_{k=1}^{N} X_{rk}^{(1)}\widetilde{u}_{xk} - a_1q\widetilde{u}_{yr} - b_1\sum_{k=1}^{N} X_{rk}^{(1)}\widetilde{w}_{xk} + b_1q\widetilde{w}_{yr} - a_4\widetilde{\sigma}_{zzr}, \\
\widetilde{\sigma}_{xyr} = a_6q\widetilde{u}_{xr} + a_6\displaystyle\sum_{k=1}^{N} X_{rk}^{(1)}\widetilde{u}_{yk} - b_1q\widetilde{w}_{xr} + b_1\sum_{k=1}^{N} X_{rk}^{(1)}\widetilde{w}_{yk}, \\
\widetilde{H}_{xxr} = b_1\displaystyle\sum_{k=1}^{N} X_{rk}^{(1)}\widetilde{u}_{xk} + b_1q\widetilde{u}_{yr} + b_2\sum_{k=1}^{N} X_{rk}^{(1)}\widetilde{w}_{xk} - b_4q\widetilde{w}_{yr}, \\
\widetilde{H}_{yyr} = b_1\displaystyle\sum_{k=1}^{N} X_{rk}^{(1)}\widetilde{u}_{xk} + b_1q\widetilde{u}_{yr} + b_4\sum_{k=1}^{N} X_{rk}^{(1)}\widetilde{w}_{xk} - b_2q\widetilde{w}_{yr}, \\
\widetilde{H}_{xyr} = -bq\widetilde{u}_{xr} - b_1\displaystyle\sum_{k=1}^{N} X_{rk}^{(1)}\widetilde{u}_{yk} + b_2q\widetilde{w}_{xr} - b_4\sum_{k=1}^{N} X_{rk}^{(1)}\widetilde{w}_{yk}, \\
\widetilde{H}_{yxr} = b_1q\widetilde{u}_{xr} + b_1\displaystyle\sum_{k=1}^{N} X_{rk}^{(1)}\widetilde{u}_{yk} - b_4q\widetilde{w}_{xr} + b_2\sum_{k=1}^{N} X_{rk}^{(1)}\widetilde{w}_{yk}.
\end{cases}
\tag{17}
$$

Three boundary conditions of SSSS, CSCS, and CSSS are considered in this paper, and the state equations which satisfy the corresponding boundary conditions are listed in Appendix A.

For the pth-layer of the plate, Eq. (16) can be written as the following unified matrix form:

$$\frac{\mathrm{d}}{\mathrm{d}z}\boldsymbol{\delta}^{(p)} = \boldsymbol{T}^{(p)}\boldsymbol{\delta}^{(p)}, \tag{18}$$

where $\boldsymbol{\delta}^{(p)} = [\boldsymbol{u}_x^{\mathrm{T}}, \boldsymbol{u}_y^{\mathrm{T}}, \boldsymbol{w}_x^{\mathrm{T}}, \boldsymbol{w}_y^{\mathrm{T}}, \boldsymbol{\sigma}_{zz}^{\mathrm{T}}, \boldsymbol{\sigma}_{xz}^{\mathrm{T}}, \boldsymbol{\sigma}_{yz}^{\mathrm{T}}, \boldsymbol{H}_{xz}^{\mathrm{T}}, \boldsymbol{H}_{yz}^{\mathrm{T}}, \boldsymbol{u}_z^{\mathrm{T}}]$ such as $\boldsymbol{u}_x^{\mathrm{T}} = \widetilde{u}_{xr}$. $\boldsymbol{T}^{(p)}$ is the coefficient matrix of the pth-layer at the appropriate discrete points. Since the elastic constant changes with the thickness, $\boldsymbol{T}^{(p)}$ is a variable coefficient matrix. At the same time, it needs to be artificially divided layers in the process of calculation, which will not lead to numerical instability[27,31] and is conducive to calculation.

According to the theory of ordinary differential equation, the solutions to Eq. (18) are derived through the propagator matrix[48–49] which connects the field variables at the upper and lower interfaces of the pth-layer,

$$\boldsymbol{\delta}^{(p)}(z) = \exp(\boldsymbol{T}^{(p)}(z - z_{p-1}))\boldsymbol{\delta}^{(p)}(z_{p-1}), \quad z_{p-1} \leqslant z \leqslant z_p. \tag{19}$$

Let $z = z_p$ in Eq. (19). We find

$$\boldsymbol{\delta}_1^{(p)+} = \boldsymbol{M}^{(p)}\boldsymbol{\delta}_0^{(p)-}, \tag{20}$$

where $\boldsymbol{M}^{(p)} = \exp((z_p - z_{p-1})\boldsymbol{T}^{(p)}) = \exp(h_p\boldsymbol{T}^{(p)})$, and "$-$" and "$+$" represent the lower and upper surfaces of the pth-layer, respectively.

If the interfaces are the perfect bonding condition, the tractions and displacements along the z-direction are continuous through this interface. Then, the propagator relation can be expressed as

$$\boldsymbol{\delta}_1^{(M)+} = \boldsymbol{P}\boldsymbol{\delta}_0^{(1)-}, \tag{21}$$

where the matrix $\boldsymbol{P} = \boldsymbol{M}^{(M)}\boldsymbol{M}^{(M-1)}\cdots\boldsymbol{M}^{(p)}\cdots\boldsymbol{M}^{(1)} = \prod_{p=M}^{1}\boldsymbol{M}^{(p)}$ is the global propagator matrix.

We rewrite Eq. (21) as follows:

$$\boldsymbol{\delta}_1^{(M)} = \begin{pmatrix}\boldsymbol{U}(H)\\ \boldsymbol{Y}(H)\end{pmatrix} = \begin{pmatrix}\boldsymbol{P}_{11} & \boldsymbol{P}_{12}\\ \boldsymbol{P}_{21} & \boldsymbol{P}_{22}\end{pmatrix}\boldsymbol{\delta}_0^{(1)} = \begin{pmatrix}\boldsymbol{P}_{11} & \boldsymbol{P}_{12}\\ \boldsymbol{P}_{21} & \boldsymbol{P}_{22}\end{pmatrix}\begin{pmatrix}\boldsymbol{U}(0)\\ \boldsymbol{Y}(0)\end{pmatrix}, \tag{22}$$

where $\boldsymbol{U}(z) = (\boldsymbol{u}_x^{\mathrm{T}}, \boldsymbol{u}_y^{\mathrm{T}}, \boldsymbol{u}_z^{\mathrm{T}}, \boldsymbol{w}_x^{\mathrm{T}}, \boldsymbol{w}_y^{\mathrm{T}})^{\mathrm{T}}$, and $\boldsymbol{Y}(z) = (\boldsymbol{\sigma}_{xz}^{\mathrm{T}}, \boldsymbol{\sigma}_{yz}^{\mathrm{T}}, \boldsymbol{\sigma}_{zz}^{\mathrm{T}}, \boldsymbol{H}_{xz}^{\mathrm{T}}, \boldsymbol{H}_{yz}^{\mathrm{T}})^{\mathrm{T}}$. According to the processing of the state space method, the total numbers of equations and unknowns in Eq. (22) for laminates with three boundary conditions need to be consistent with those of Appendix A, respectively. For example, the total numbers of equations and unknowns in Appendix A for the laminate with boundary condition CSCS are both $10N - 20$.

It is assumed that the mechanical boundary conditions on the top and bottom surfaces of the plate can be expressed as

$$\begin{cases}\boldsymbol{\sigma}_{xz}^{\mathrm{T}} = \boldsymbol{\sigma}_{yz}^{\mathrm{T}} = \boldsymbol{H}_{xz}^{\mathrm{T}} = \boldsymbol{H}_{yz}^{\mathrm{T}} = \boldsymbol{0}, \quad \boldsymbol{\sigma}_{zz}^{\mathrm{T}} = \boldsymbol{\sigma}_0^{\mathrm{T}}\sin(qy) \quad \text{at} \quad z = H,\\ \boldsymbol{\sigma}_{zz}^{\mathrm{T}} = \boldsymbol{\sigma}_{xz}^{\mathrm{T}} = \boldsymbol{\sigma}_{yz}^{\mathrm{T}} = \boldsymbol{H}_{xz}^{\mathrm{T}} = \boldsymbol{H}_{yz}^{\mathrm{T}} = \boldsymbol{0} \quad \text{at} \quad z = 0,\end{cases} \tag{23}$$

where

$$\boldsymbol{\sigma}_0^{\mathrm{T}} = (\sigma_0\sin(\pi x_2/L_x), \cdots, \sigma_0\sin(\pi x_r/L_x), \cdots, \sigma_0\sin(\pi x_{N-1}/L_x))^{\mathrm{T}}, \quad 2 \leqslant r \leqslant N-1 \tag{24}$$

with the load amplitude σ_0.

Incorporating Eq. (23) with Eq. (22) yields

$$\boldsymbol{\delta}_1^{(M)} = \begin{pmatrix} \boldsymbol{U}(H) \\ \boldsymbol{Y}(H) \end{pmatrix} = \begin{pmatrix} \boldsymbol{P}_{11} & \boldsymbol{P}_{12} \\ \boldsymbol{P}_{21} & \boldsymbol{P}_{22} \end{pmatrix} \boldsymbol{\delta}_0^{(1)} = \begin{pmatrix} \boldsymbol{P}_{11} & \boldsymbol{P}_{12} \\ \boldsymbol{P}_{21} & \boldsymbol{P}_{22} \end{pmatrix} \begin{pmatrix} \boldsymbol{U}(0) \\ \boldsymbol{0} \end{pmatrix}, \tag{25}$$

where $\boldsymbol{Y}(H) = (\boldsymbol{0}, \boldsymbol{0}, \boldsymbol{\sigma}_{zz}^{\mathrm{T}}, \boldsymbol{0}, \boldsymbol{0})^{\mathrm{T}}$. Then, the solution of the FG 2D QC plate can be obtained through Eq. (25).

3 Numerical examples

In this section, the layered FGM plate subject to a normal force at the top surface with different boundary conditions is studied. The laminate is composed of three single plates, and each layer has an equal thickness. The horizontal dimensions of this FG QC plate are $L_x \times L_y = 10\,\mathrm{mm} \times 10\,\mathrm{mm}$, and its total thickness is $H = 3\,\mathrm{mm}$. We fix the load amplitude $\sigma_0 = 1\,\mathrm{N/m^2}$ and the superposition $n = 1$ in Eq. (10). Meanwhile, the discrete points are taken as $N = 13$. Two kinds of materials are considered[44,47]. One is the QC material Al-Ni-Co (called QC), and the other is the crystal material $BaTiO_3$ (called C). The material properties for Al-Ni-Co and $BaTiO_3$ are listed in Table 1. For the FGM plate, we assume that the middle layer is homogeneous, and the material properties of the top and bottom layers are symmetric exponential distribution along the z-direction, as shown in Fig. 2. Five different exponential factors, i.e., $\eta = -0.4, -0.2$, 0.0, 0.2, and 0.4, are studied. The crystal material $BaTiO_3$ lacks the phason field. In order to avoid the appearance of a singular matrix in the calculation process, we assume that the phason elastic constant K_i of the crystal is 10^{-8} times that of the QC[44].

Table 1 Material properties ($\boldsymbol{C}^0$ in 10^9 N/m^2, $\boldsymbol{K}^0$ in 10^9 N/m^2, $\boldsymbol{R}^0$ in 10^8 N/m^2)

Material	C_{11}^0	C_{12}^0	C_{13}^0	C_{33}^0	C_{44}^0	K_1^0	K_2^0	K_4^0	R_1^0
Al-Ni-Co	234.33	57.41	66.63	232.22	70.19	122	24	12	8.846
$BaTiO_3$	166	77	78	162	43				

3.1 Validation

In this part, we present one numerical example of the QC/QC/QC plate to verify the validity and accuracy of the proposed method and the numerical solution. In the calculation process, the FG exponential factors are fixed at $\eta = 0$, and the horizontal coordinate is fixed at $(x, y) = (0.75L_x, 0.75L_y)$. Furthermore, the material parameters, the shape and size of the plate, and the mechanical quantities used are consistent with those in Ref. [37]. The phonon displacement, the phason displacement, the phonon stress, and the phason stress are normalized by their maximum values among these four variables along the thickness direction.

Figure 3 shows the variations of the displacements and stresses of phonon and phason fields for the QC/QC/QC plate with the boundary condition SSSS under the mechanical load. It can be proved that the solutions based on the SS-DQM are in good agreement with the results by Yang et al.[37], as shown in Fig. 3. Therefore, the method in this paper has high precision and good convergence. Furthermore, when the discrete points are taken as $N = 9$, the maximal relative error of the present solution is only about 0.001% for the solution in Ref. [37]. With the increase in the discrete points N, this solution becomes more accurate. However, by comparing the calculation results, when $N \geqslant 21$, numerical instability is encountered. Thus, to ensure the accuracy and convergence of the solution, the discrete points are taken as $N = 13$ in the following examples. It should be mentioned that the numerical instabilities are always encountered during the present solution procedure in the case of high aspect ratio of H/L_y, large discrete point number, and high-order frequencies[27]. In this paper, since $H/L_y = 0.3$ and $N = 13$, the solutions are stable.

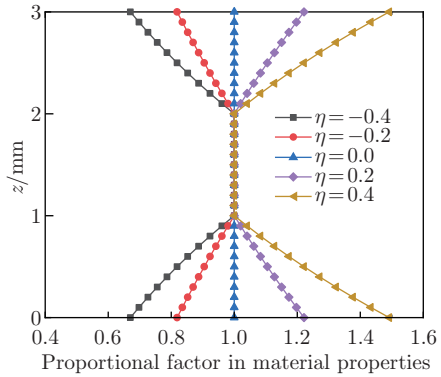

Fig. 2 Variations of the FGM proportional factors for $\eta = -0.4, -0.2, 0.0, 0.2,$ and 0.4 (color online)

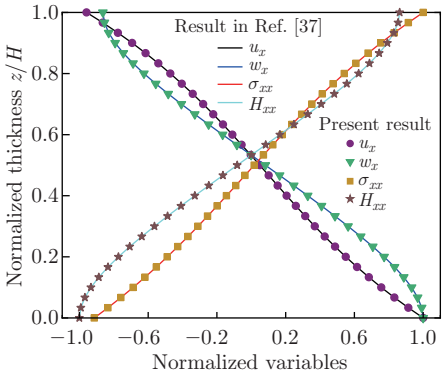

Fig. 3 Normalized displacements and stresses for the QC/QC/QC plate (color online)

3.2 FG QC laminate with boundary condition SSSS

In this part, we present the solution of the C/QC/C plate with the boundary condition SSSS. The FG exponential factors are set as $\eta = -0.4, -0.2, 0.0, 0.2,$ and 0.4. The horizontal coordinate is fixed at $(x, y) = (0.75L_x, 0.75L_y)$.

The variations of the displacements and stresses for the C/QC/C plate along the thickness direction under the mechanical load are presented in Fig. 4. With the increase in the FG exponential factors, the absolute maximum values of the field variables (see Figs. 4(a)–4(e)) for the FG QC laminates decrease continuously. The magnitude of u_x ($u_x = u_y$) in Fig. 4(a) is much larger than that of w_x ($w_x = -w_y$) in Fig. 4(b). Since we did not use the plane assumption in the 2D theory of thick plate bending, the distributions of σ_{xz} (see Fig. 4(c)) and H_{xz} (see Fig. 4(d)) are nonlinear. Corresponding to u_x and w_x, the similar relationships of stresses are $\sigma_{xz} = \sigma_{yz}$ and $H_{xz} = -H_{yz}$, respectively.

3.3 FG QC laminate with boundary condition CSCS

In this part, we present the solution of the QC/C/QC plate with the boundary condition CSCS. The FG exponential factors are set as $\eta = -0.4, -0.2, 0.0, 0.2,$ and 0.4. To show the distribution of field variables along the z-direction, the horizontal coordinate is fixed at $(x, y) = (0.25L_x, 0.5L_y)$.

The variations of the phonon and phason displacements for the QC/C/QC plate along the thickness direction under the mechanical load are presented in Fig. 5. With the increase in the FG exponential factor η, the absolute values of the field variables (see Figs. 5(a)–5(d)) on the upper and lower surfaces of the plate decrease continuously. The values of u_x (see Fig. 5(a)) and u_y are not equal due to different boundary conditions on the four edges. Furthermore, the distribution of u_x along the thickness direction changes explicitly rather than linear or polynomial form as assumed in the thin plate theory and the thick plate theory. The values of u_z (see Fig. 5(b)) of the upper and lower surfaces are different for the QC/C/QC plate, indicating that the extrusion deformation cannot be ignored. w_x and w_y (see Figs. 5(c) and 5(d)) vary nonlinearly in the QC layer and return to zero in the crystal layer due to the fact that the phason coefficients are almost zero for the material $BaTiO_3$, and this transformation can be used to identify the stacking sequence of materials.

The variations of the phonon and phason stresses for the QC/C/QC plate along the thickness direction under the mechanical load are presented in Fig. 6. The value of σ_{xz} (see Fig. 6(a)) increases with the increase in η. When the horizontal coordinate is fixed at $(x, y) = (0.25L_x, 0.5L_y)$, the value of σ_{zz} (see Fig. 6(b)) on the upper surface is 0.707 11, and its distribution changes

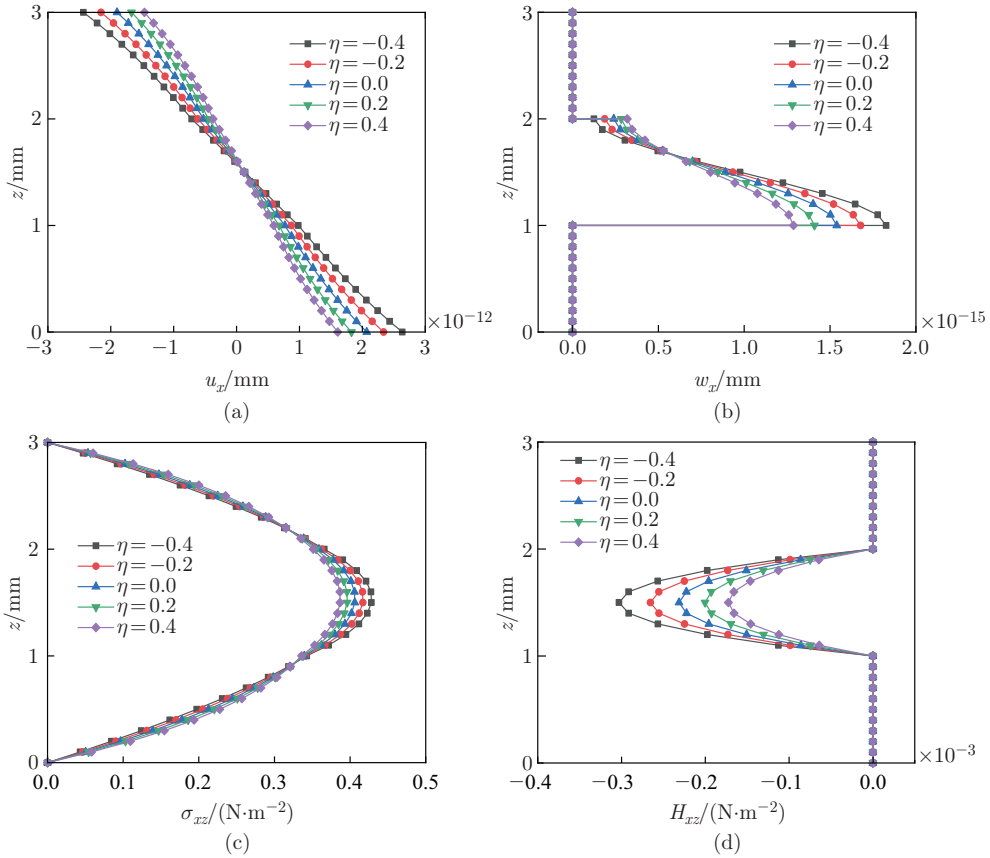

Fig. 4 Displacements and stresses for the C/QC/C plate: (a) u_x, (b) w_x, (c) σ_{xz}, and (d) H_{xz} (color online)

slightly with the increase in η. The phonon stress σ_{xx} is discontinuous between different material layers in Fig. 6(c). Based on the classic laminate theory, only the local stress of the basic equation of the QC is considered. However, in fact, the stress state also includes the strong interlayer stress between the interfaces. The high-interlayer stress is considered to be one of the special failure mechanisms of composite materials in engineering applications. The values of H_{xz} for the QC/C/QC plate in Fig. 6(d) are zero in the crystal layers and change with varying η from -0.4 to 0.4 in the QC layer. With the increase in η, the values of H_{yz} (see Fig. 6(e)) in the QC layer increase continuously. H_{xx} (see Fig. 6(f)) is discontinuous at $z = 1\,\text{mm}$ or $z = 2\,\text{mm}$, and the interlayer stress value decreases with the increase in η.

3.4 FG QC laminate with boundary condition CSSS

In this part, we present the solutions of five kinds of stacking sequence plates (QC/QC/QC, C/QC/QC, QC/C/QC, C/QC/C, and QC/C/C) with the boundary condition CSSS. The FG exponential factors are set as $\eta = 0$. To show the distribution of field variables along the z-direction, the horizontal coordinate is fixed at $(x, y) = (L_x, 0.5L_y)$.

The variations of the phonon and phason displacements for laminates along the thickness direction under the mechanical load are presented in Fig. 7. It can be observed that u_x (see Fig. 7(a)) is continuous at the interface between layers. Furthermore, the stacking sequence has few effects on u_x. The stacking sequence does not change the magnitude and direction of u_x at the upper and lower surfaces of the laminates. The stacking sequences have an apparent effect

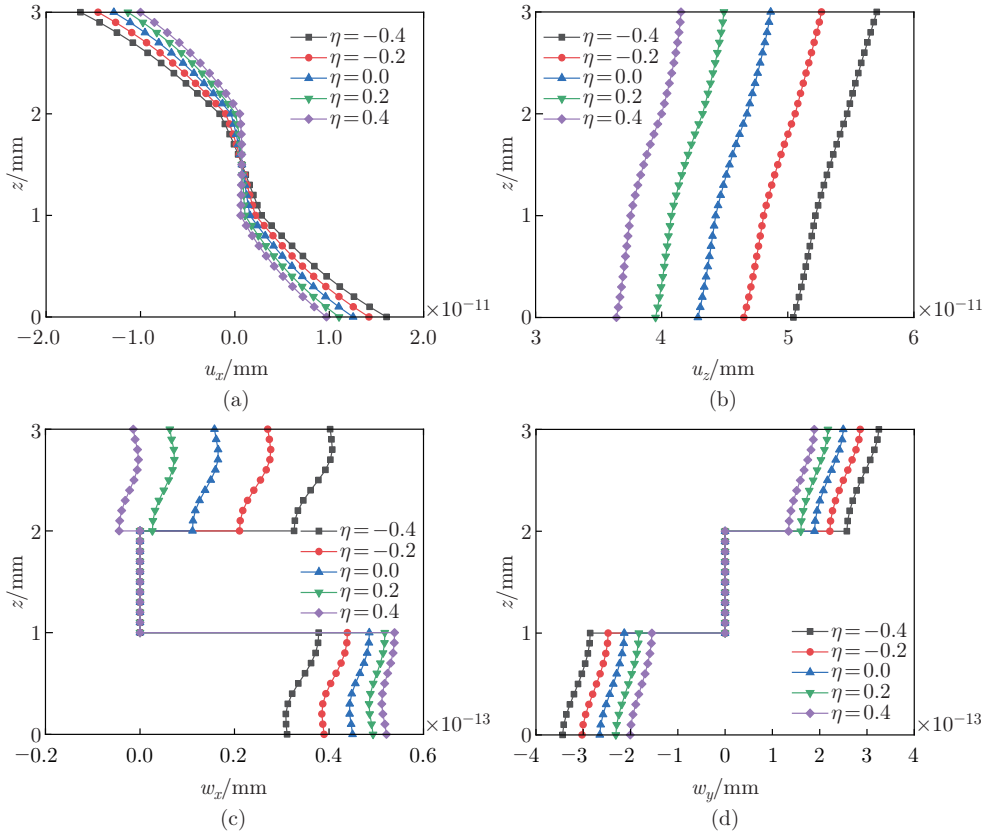

Fig. 5 Phonon and phason displacements for the QC/C/QC plate: (a) u_x, (b) u_z, (c) w_x, and (d) w_y (color online)

on w_x (see Fig. 7(b)), and w_x is zero in the crystal layer.

The variations of the phonon and phason stresses for laminates along the thickness direction under the mechanical load are presented in Fig. 8. According to the classic laminate theory, the stresses at the edge of the plate cannot be calculated. However, Figs. 8(a)–8(d) present the accurate stress solutions on simply supported edges, which also indicate that these solutions are of theoretical significance. The distributions of σ_{xz} and H_{xz} along the z-direction are not symmetrical in Figs. 8(a) and 8(b). The distribution of these stresses at $x = L_x$ is consistent with the in-plane distribution trend, and the value is larger at the boundary. σ_{xy} (see Fig. 8(c)) is the same as σ_{xx} and σ_{yy}, which is discontinuous between different material layers. If the material properties of each layer are the same, the stress is continuous for the QC/QC/QC plate. Similarly, H_{yx} (see Fig. 8(d)) is continuous between two adjacent QC material layers. For the above physical variables, if the DQM will be also utilized to discretize domains along the y-direction, the superposition n will not appear in the formulations of the exact solution.

3.5 FG QC laminate with boundary conditions SSSS, CSCS, and CSSS

In this part, we present the solutions of the QC/C/QC plate with different boundary conditions (SSSS, CSCS, and CSSS) and let $\eta = 0.2$. The horizontal coordinate is fixed at $(x, y) = (0.25L_x, 0.5L_y)$.

The variations of the phonon and phason displacements for the QC/C/QC plate along the thickness direction under the mechanical load are presented in Fig. 9. It can be observed that the boundary condition SSSS has greater effects on u_y (see Fig. 9(a)) and w_y (see Fig. 9(b)) than

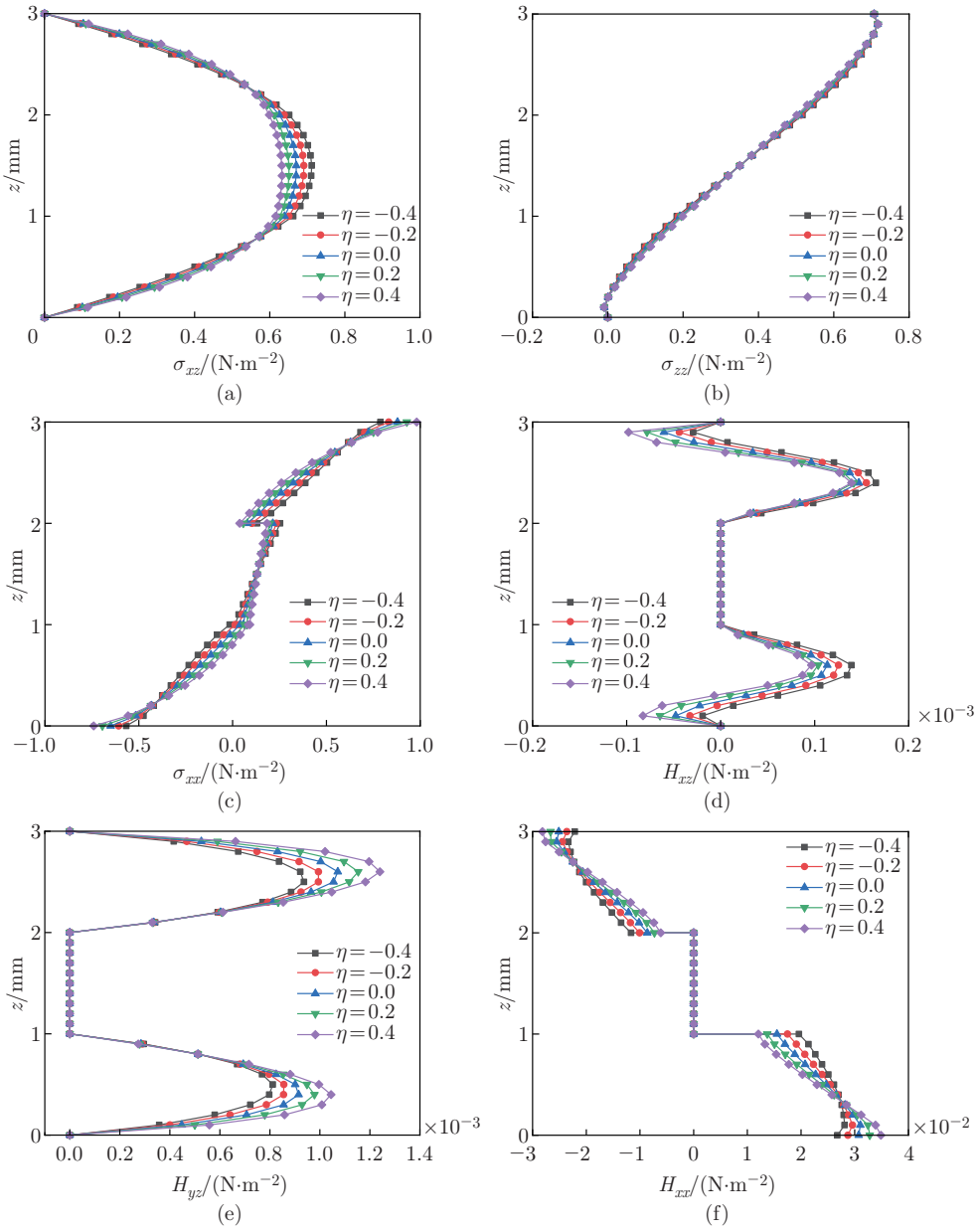

Fig. 6 Phonon and phason stresses for the QC/C/QC plate: (a) σ_{xz}, (b) σ_{zz}, (c) σ_{xx}, (d) H_{xz}, (e) H_{yz}, and (f) H_{xx} (color online)

CSCS. This feature indicates that CSCS can bear a greater load. Furthermore, the values of u_y and w_y decrease with the increase in the number of clamped supported edges. This feature is in accord with the law of displacement in elasticity theory.

The variations of the phonon and phason stresses for the QC/C/QC along the thickness direction under the mechanical load are presented in Fig. 10. The values of σ_{yz} and H_{yz} (see Figs. 10(a) and 10(b)) with the boundary condition SSSS are greater than those of σ_{yz} and H_{yz} with CSCS or CSSS. This feature indicates that the clamped supported boundary conditions are more constrained than the simply supported edge for the phason stresses, and it can bear

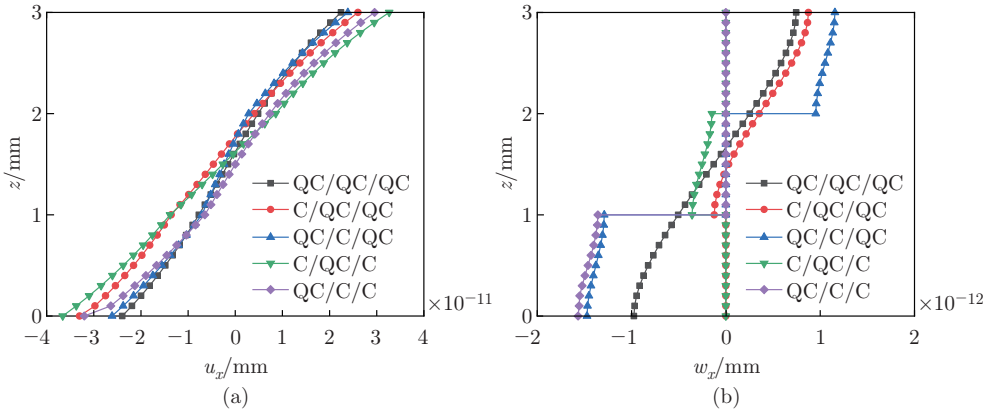

Fig. 7 Phonon and phason displacements for the QC laminates: (a) u_x and (b) w_x (color online)

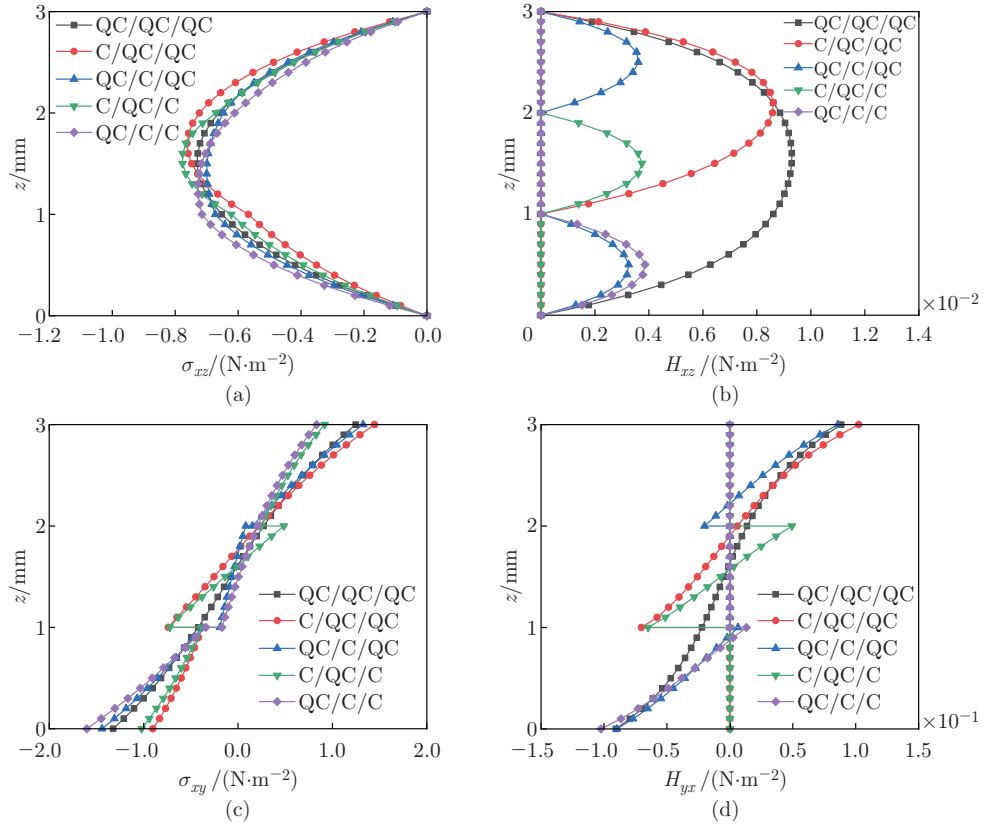

Fig. 8 Phonon and phason stresses for the QC laminates: (a) σ_{xz}, (b) H_{xz}, (c) σ_{xy}, and (d) H_{yx} (color online)

more load. σ_{yy} (see Fig. 10(c)) is continuous at $z = 1\,\text{mm}$ and $z = 2\,\text{mm}$, and the value of the interlayer stress at $z = 2\,\text{mm}$ is smaller than that of the interlayer stress at $z = 1\,\text{mm}$. Similarly, when the horizontal coordinate is fixed at $(x, y) = (0.25L_x, 0.5L_y)$, the value of σ_{zz} (see Fig. 10(d)) on the upper surface is 0.707 11, whose distribution is almost unchanged with three boundary conditions.

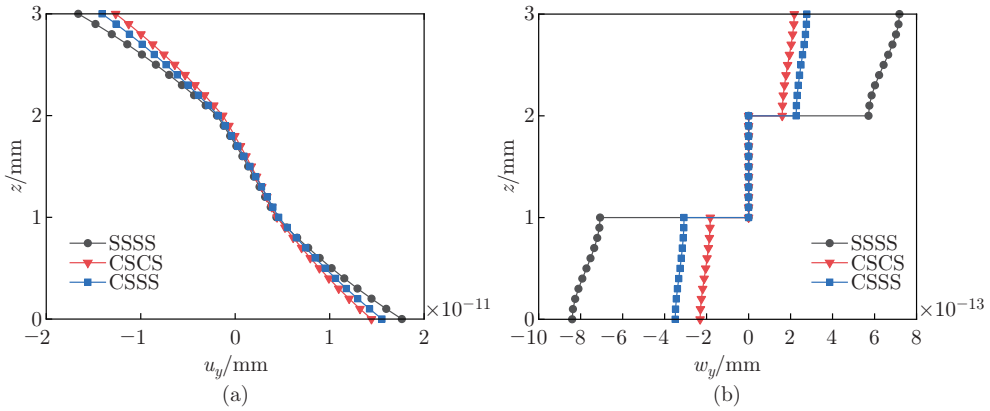

Fig. 9 Phonon and phason displacements for the QC/C/QC plate: (a) u_y and (b) w_y (color online)

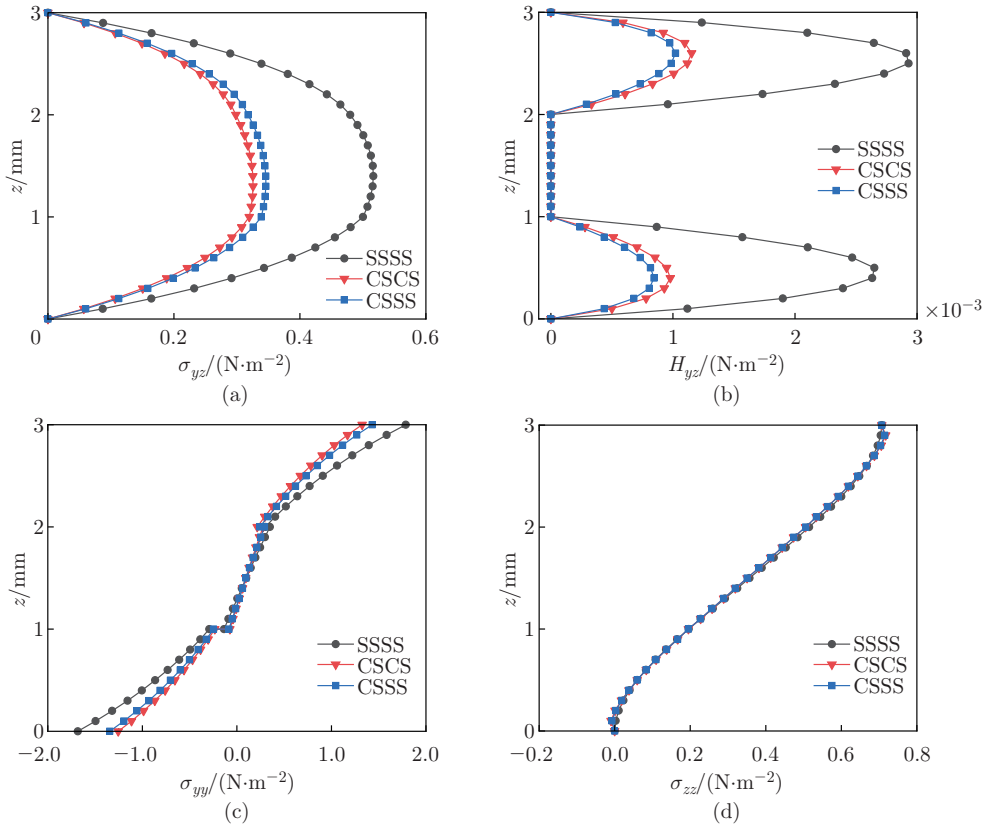

Fig. 10 Phonon and phason stresses for the QC/C/QC plate: (a) σ_{yz}, (b) H_{yz}, (c) σ_{yy}, and (d) σ_{zz} (color online)

4 Conclusions

In this paper, the semi-analytical SS-DQM, which is composed of the differential quadrature equations and the state-space method, is constructed to obtain the solution of the static response of the FG multilayered 2D decagonal QC rectangular plates with mixed boundary conditions.

The differential quadrature technique is used to discretize the in-plane domains, from which the simply supported and clamped supported boundary conditions can be directly processed. At the same time, the thickness direction is analytically solved utilizing the propagator matrix method and the state-space method. Therefore, this semi-analytical method inherits the advantages of the two methods, such as high accuracy, rapid convergence, and capability of treating mixed constraint conditions directly. These advantages of this method are verified in the numerical examples. Finally, some significant features are listed below.

(i) The distributions of the phonon and phason displacements along the thickness direction change explicitly rather than the linear or polynomial form as assumed in the thin plate theory and the thick plate theory of plate bending.

(ii) σ_{xx}, σ_{yy}, σ_{xy}, H_{xx}, H_{yy}, and H_{yz} are discontinuous at the interface between the layers when the materials of two adjacent layers of the laminated board are different. This interface stress discontinuity is affected by the strong interlayer stress.

(iii) The values of the variables in the phonon and phason fields vary with η. All comparison studies for the stacking sequence reveal the obvious effect of it on the physical fields, especially at the interfaces of the FG multilayered plate.

(iv) The clamped supported boundary conditions have few effects on the phonon and phason interlayer stresses. The clamped supported boundary conditions are also more constrained than the simply supported edge for the phason stresses.

The semi-analytical method constructed in this paper has high precision and fast convergence for deriving the solutions of the FG 2D QC laminates with mixed boundary conditions. Some special cases such as the multi-field coupled QC, FG 1D and 3D QC, and piezoelectric QC plates could all be investigated according to the present solutions. Furthermore, the methods and numerical results in this paper can be utilized to verify the accuracy of other numerical methods and serve for the analysis and design of intelligent QC material laminates.

References

[1] SHECHTMAN, D. G., BLECH, I. A., GRATIAS, D., and CAHN, J. W. Metallic phase with long-range orientational order and no translational symmetry. *Physical Review Letters*, **53**, 1951–1953 (1984)

[2] FAN, T. Y. and GUO, Y. C. Mathematical methods for a class of mixed boundary-value problems of planar pentagonal quasicrystal and some solutions. *Science in China Series A*: *Mathematics*, **40**, 990–1003 (1997)

[3] FAN, T. Y. Mathematical theory and methods of mechanics of quasicrystalline materials. *Engineering*, **5**, 407–448 (2013)

[4] GUO, J. H. and LIU, G. T. Analytic solutions to problem of elliptic hole with two straight cracks in one-dimensional hexagonal quasicrystals. *Applied Mathematics and Mechanics* (*English Edition*), **29**(4), 485–493 (2008) https://doi.org/10.1007/s10483-008-0406-x

[5] FLEURY, E., LEE, S. M., KIM, W. T., and KIM, D. H. Effects of air plasma spraying parameters on the Al-Cu-Fe quasicrystalline coating layer. *Journal of Non-Crystalline Solids*, **278**, 194–204 (2000)

[6] DUBOIS, J. M. Properties and applications of quasicrystals and complex metallic alloys. *Chemical Society Reviews*, **41**, 6760–6777 (2012)

[7] TIAN, Y., HUANG, H., YUAN, G. Y., and DING, W. J. Microstructure evolution and mechanical properties of quasicrystal-reinforced Mg-Zn-Gd alloy processed by cyclic extrusion and compression. *Journal of Alloys and Compounds*, **626**, 42–48 (2015)

[8] LI, X. Y., WANG, T., ZHENG, R. F., and KANG, G. Z. Fundamental thermo-electro-elastic solutions for 1D hexagonal QC. *Journal of Applied Mathematics and Mechanics*, **95**, 457–468 (2015)

[9] PAN, E. Exact solution for functionally graded anisotropic elastic composite laminates. *Journal of Composite Materials*, **37**, 1903–1920 (2003)

[10] PAN, E. and HAN, F. Exact solution for functionally graded and layered magneto-electro-elastic plates. *International Journal of Engineering Science*, **43**, 321–339 (2005)

[11] YAS, M. H. and RAHIMI, S. Thermal vibration of functionally graded porous nanocomposite beams reinforced by graphene platelets. *Applied Mathematics and Mechanics* (*English Edition*), **41**(8), 1209–1226 (2020) https://doi.org/10.1007/s10483-020-2634-6

[12] GUO, J. H., CHEN, J. Y., and PAN, E. A three-dimensional size-dependent layered model for simply-supported and functionally graded magnetoelectroelastic plates. *Acta Mechanica Solida Sinica*, **31**, 652–671 (2018)

[13] GUO, J. H., CHEN, J. Y., and PAN, E. Size-dependent behavior of functionally graded anisotropic composite plates. *International Journal of Engineering Science*, **106**, 110–124 (2016)

[14] MATSUNAGA, H. Free vibration and stability of functionally graded shallow shells according to a 2D higher-order deformation theory. *Composite Structures*, **84**, 132–146 (2008)

[15] HUANG, Z. Y., LU, C. F., and CHEN, W. Q. Benchmark solutions for functionally graded thick plates resting on Winkler-Pasternak elastic foundations. *Composite Structures*, **85**, 95–104 (2008)

[16] LU, C. F., LIM, C. W., and CHEN, W. Q. Exact solutions for free vibrations of functionally graded thick plates on elastic foundations. *Mechanics of Composite Materials Structures*, **16**, 576–584 (2009)

[17] YING, J., LU, C. F., and LIM, C. W. 3D thermoelasticity solutions for functionally graded thick plates. *Journal of Zhejiang University-SCIENCE A*, **10**, 327–336 (2009)

[18] HUANG, Y. Z., LI, Y., YANG, L. Z., and GAO, Y. Static response of functionally graded multilayered one-dimensional hexagonal piezoelectric quasicrystal plates using the state vector approach. *Journal of Zhejiang University-SCIENCE A*, **20**, 133–147 (2019)

[19] ZHANG, L., GUO, J. H., and XING, Y. M. Nonlocal analytical solution of functionally graded multilayered one-dimensional hexagonal piezoelectric quasicrystal nanoplates. *Acta Mechanica*, **230**, 1781–1810 (2019)

[20] LI, Y., YANG, L. Z., and GAO, Y. An exact solution for a functionally graded multilayered one-dimensional orthorhombic quasicrystal plate. *Acta Mechanica*, **230**, 1257–1273 (2017)

[21] LI, Y., YANG, L. Z., and GAO, Y. Thermo-elastic analysis of functionally graded multilayered two-dimensional decagonal quasicrystal plates. *Journal of Applied Mathematics and Mechanics*, **98**, 1585–1602 (2018)

[22] LI, Y., YANG, L. Z., and GAO, Y. Bending analysis of laminated two-dimensional piezoelectric quasicrystal plates with functionally graded material properties. *Acta Physica Polonica A*, **135**, 426–433 (2019)

[23] BALUBAID, M., TOUNSI, A., DAKHEL, B., and MAHMOUD, S. R. Free vibration investigation of FG nanoscale plate using nonlocal two variables integral refined plate theory. *Computers and Concrete*, **24**, 579–586 (2019)

[24] ZHANG, B., YU, J. G., and ZHANG, X. M. Guided wave propagation in functionally graded one-dimensional hexagonal quasi-crystal plates. *Journal of Mechanics*, **36**, 773–788 (2020)

[25] RUOCCO, E. and MINUTOLO, V. Buckling of composite plates with arbitrary boundary conditions by a semi-analytical approach. *International Journal of Structural Stability and Dynamics*, **12**, 347–363 (2012)

[26] CUI, J., LI, Z. C., YE, R. C., JIANG, W. A., and TAO, S. H. A semianalytical three-dimensional elasticity solution for vibrations of orthotropic plates with arbitrary boundary conditions. *Shock and Vibration*, **2019**, 1–20 (2019)

[27] LU, C. F., CHEN, W. Q., and SHAO, J. W. Semi-analytical three-dimensional elasticity solutions for generally laminated composite plates. *European Journal of Mechanics-A/Solids*, **27**, 899–917 (2008)

[28] WANG, X. W. Differential quadrature in the analysis of structural components. *Advances in Mechanics*, **25**, 232–240 (1995)

[29] ZHOU, Y. Y., CHEN, W. Q., LU, C. F., and WANG, J. Free vibration of cross-ply piezoelectric laminates in cylindrical bending with arbitrary edges. *Composite Structures*, **87**, 93–100 (2009)

[30] BELLMAN, R., CASTI, J., and KASHEF, B. G. Differential quadrature: a technique for the rapid solution of nonlinear partial differential equations. *Journal of Computational Physics*, **10**, 40–52 (1972)

[31] ZHOU, Y. Y., CHEN, W. Q., and LU, C. F. Semi-analytical solution for orthotropic piezoelectric laminates in cylindrical bending with interfacial imperfections. *Composite Structures*, **92**, 1009–1018 (2010)

[32] YAS, M. H., JODAEI, A., IRANDOUST, S., and AGHDAM, M. N. Three-dimensional free vibration analysis of functionally graded piezoelectric annular plates on elastic foundations. *Meccanica*, **47**, 1401–1423 (2012)

[33] YAS, M. H. and MOLOUDI, N. Three-dimensional free vibration analysis of multi-directional functionally graded piezoelectric annular plates on elastic foundations via state space based differential quadrature method. *Applied Mathematics and Mechanics* (*English Edition*), **36**(4), 439–464 (2015) https://doi.org/10.1007/s10483-015-1923-9

[34] LI, L. H. and YUN, G. H. Elastic fields around a nanosized elliptic hole in decagonal quasicrystals. *Chinese Physics B*, **23**, 1–6 (2014)

[35] ZHAO, M. H., FAN, C. Y., LU, C. S., and DANG, H. Y. Analysis of interface cracks in one-dimensional hexagonal quasi-crystal coating under in-plane loads. *Engineering Fracture Mechanics*, **243**, 107534 (2021)

[36] YANG, D. S. and LIU, G. T. Anti-plane problem of nano-cracks emanating from a regular hexagonal nano-hole in one-dimensional hexagonal piezoelectric quasicrystals. *Chinese Physics B*, **29**, 104601 (2020)

[37] YANG, L. Z., GAO, Y., PAN, E., and WAKSMANSKI, N. An exact solution for a multilayered two-dimensional decagonal quasicrystal plate. *International Journal of Solids and Structures*, **51**, 1737–1749 (2014)

[38] ZHANG, L. L., ZHANG, Y. M., and GAO, Y. General solutions of plane elasticity of one-dimensional orthorhombic quasicrystals with piezoelectric effect. *Physics Letters A*, **378**, 2768–2776 (2014)

[39] LI, Y., QIN, Q. H., and ZHAO, M. H. Analysis of 3D planar crack problems of one-dimensional hexagonal piezoelectric quasicrystals with thermal effect, part II: numerical approach. *International Journal of Solids and Structures*, **188**, 223–232 (2020)

[40] LI, Y., QIN, Q. H., and ZHAO, M. H. Analysis of 3D planar crack problems in one-dimensional hexagonal piezoelectric quasicrystals with thermal effect, part I: theoretical formulations. *International Journal of Solids and Structures*, **188**, 269–281 (2020)

[41] DING, D. H., YANG, W. G., HU, C. Z., and WANG, R. H. Generalized elasticity theory of quasicrystals. *Physical Review B*, **48**, 7003–7010 (1993)

[42] HU, C. Z., WANG, R. H., and DING, D. H. Symmetry groups, physical property tensors, elasticity and dislocations in quasicrystals. *Reports on Progress in Physics*, **63**, 1–39 (2000)

[43] HU, C. Z., WANG, R. H., DING, D. H., and YANG, W. G. Piezoelectric effects in quasicrystals. *Physical Review B*, **56**, 2463–2468 (1997)

[44] LI, Y., YANG, L. Z., ZHANG, L. L., and GAO, Y. Size-dependent effect on functionally graded multilayered two-dimensional quasicrystal nanoplates under patch/uniform loading. *Acta Mechanica*, **229**, 3501–3515 (2018)

[45] NIE, G. J. and ZHONG, Z. Semi-analytical solution for three-dimensional vibration of functionally graded circular plates. *Computer Methods in Applied Mechanics and Engineering*, **196**, 4901–4910 (2007)

[46] BERT, C. W. and MALIK, M. Differential quadrature method in computational mechanics: a review. *Applied Mechanics Reviews*, **49**, 1–28 (1996)

[47] GAO, Y. and ZHAO, B. S. General solutions of three-dimensional problems for two-dimensional quasicrystals. *Applied Mathematical Modelling*, **33**, 3382–3391 (2009)

[48] PESTEL, E. C. and LECKIE, F. A. *Matrix Methods in Elastomechanics*, McGraw-Hill, London (1963)

[49] GILBERT, K. E. A propagator matrix method for periodically stratified media. *The Journal of the Acoustical Society of America*, **73**, 137–142 (1983)

Appendix A

Some parameters are

$$a_1 = C_{11}^0 - \frac{C_{13}^0 C_{13}^0}{C_{33}^0}, \quad a_2 = \frac{1}{C_{44}^0}, \quad a_3 = C_{12}^0 - \frac{C_{12}^0 C_{23}^0}{C_{33}^0}, \quad a_4 = -\frac{C_{13}^0}{C_{33}^0},$$
$$a_5 = \frac{1}{C_{33}^0}, \quad a_6 = C_{66}^0, \quad b_1 = R_1^0, \quad b_2 = K_1^0, \quad b_3 = \frac{1}{K_4^0}, \quad b_4 = K_2^0.$$

The state equations for SSSS are

$$\frac{\mathrm{d}\widetilde{u}_{xr}}{\mathrm{d}z} = a_2\widetilde{\sigma}_{xzr} - \sum_{k=2}^{N-1} X_{rk}^{(1)}\widetilde{u}_{zk} \quad (1 \leqslant r \leqslant N), \quad \frac{\mathrm{d}\widetilde{u}_{yr}}{\mathrm{d}z} = a_2\widetilde{\sigma}_{yzr} - q\widetilde{u}_{zr} \quad (2 \leqslant r \leqslant N-1),$$

$$\frac{\mathrm{d}\widetilde{w}_{xr}}{\mathrm{d}z} = b_3\widetilde{H}_{xzr} \quad (1 \leqslant r \leqslant N), \quad \frac{\mathrm{d}\widetilde{w}_{yr}}{\mathrm{d}z} = b_3\widetilde{H}_{yzr} \quad (2 \leqslant r \leqslant N-1),$$

$$\frac{\mathrm{d}\widetilde{\sigma}_{zzr}}{\mathrm{d}z} = -\sum_{k=1}^{N} X_{rk}^{(1)}\widetilde{\sigma}_{xzk} + q\widetilde{\sigma}_{yzr} \quad (2 \leqslant r \leqslant N-1),$$

$$\begin{aligned}\frac{\mathrm{d}\widetilde{\sigma}_{xzr}}{\mathrm{d}z} = {} & -a_1\sum_{k=1}^{N}(X_{rk}^{(2)} - f_{rk})\widetilde{u}_{xk} + a_6q^2\widetilde{u}_{xr} + (a_3+a_6)q\sum_{k=2}^{N-1} X_{rk}^{(1)}\widetilde{u}_{yk} - b_1\sum_{k=1}^{N}(X_{rk}^{(2)} - f_{rk})\widetilde{w}_{xk} \\ & - b_1q^2\widetilde{w}_{xr} + 2b_1q\sum_{k=2}^{N-1} X_{rk}^{(1)}\widetilde{w}_{yk} + a_4\sum_{k=2}^{N-1} X_{rk}^{(1)}\widetilde{\sigma}_{zzk} \quad (1 \leqslant r \leqslant N),\end{aligned}$$

$$\begin{aligned}\frac{\mathrm{d}\widetilde{\sigma}_{yzr}}{\mathrm{d}z} = {} & -(a_3+a_6)q\sum_{k=1}^{N} X_{rk}^{(1)}\widetilde{u}_{xk} - a_6\sum_{k=2}^{N-1} X_{rk}^{(2)}\widetilde{u}_{yk} + a_1q^2\widetilde{u}_{yr} \\ & + 2b_1q\sum_{k=1}^{N} X_{rk}^{(1)}\widetilde{w}_{xk} - b_1\sum_{k=2}^{N-1} X_{rk}^{(2)}\widetilde{w}_{yk} - b_1q^2\widetilde{w}_{yr} + a_4q\widetilde{\sigma}_{zzr} \quad (2 \leqslant r \leqslant N-1),\end{aligned}$$

$$\frac{\mathrm{d}\widetilde{H}_{xzr}}{\mathrm{d}z} = -b_1\sum_{k=1}^{N} X_{rk}^{(2)}\widetilde{u}_{xk} - b_1q^2\widetilde{u}_{xr} - 2b_1q\sum_{k=2}^{N-1} X_{rk}^{(1)}\widetilde{u}_{yk} - b_2\sum_{k=1}^{N} X_{rk}^{(2)}\widetilde{w}_{xk} + b_2q^2\widetilde{w}_{xr} \quad (1 \leqslant r \leqslant N),$$

$$\begin{aligned}\frac{\mathrm{d}\widetilde{H}_{yzr}}{\mathrm{d}z} = {} & -2b_1q\sum_{k=1}^{N} X_{rk}^{(1)}\widetilde{u}_{xk} - b_1\sum_{k=2}^{N-1} X_{rk}^{(2)}\widetilde{u}_{yk} - b_1q^2\widetilde{u}_{yr} \\ & - b_2\sum_{k=2}^{N-1} X_{rk}^{(2)}\widetilde{w}_{yk} + b_2q^2\widetilde{w}_{yr} \quad (2 \leqslant r \leqslant N-1),\end{aligned}$$

$$\frac{\mathrm{d}\widetilde{u}_{zr}}{\mathrm{d}z} = a_4\sum_{k=1}^{N} X_{rk}^{(1)}\widetilde{u}_{xk} - a_4q\widetilde{u}_{yr} + a_5\widetilde{\sigma}_{zzr} \quad (2 \leqslant r \leqslant N-1).$$

The state equations for CSCS are

$$\frac{\mathrm{d}\widetilde{u}_{xr}}{\mathrm{d}z} = a_2\widetilde{\sigma}_{xzr} - \sum_{k=2}^{N-1} X_{rk}^{(1)}\widetilde{u}_{zk}, \quad \frac{\mathrm{d}\widetilde{u}_{yr}}{\mathrm{d}z} = a_2\widetilde{\sigma}_{yzr} - q\widetilde{u}_{zr}, \quad \frac{\mathrm{d}\widetilde{w}_{xr}}{\mathrm{d}z} = b_3\widetilde{H}_{xzr},$$

$$\frac{\mathrm{d}\widetilde{w}_{yr}}{\mathrm{d}z} = b_3\widetilde{H}_{yzr}, \quad \frac{\mathrm{d}\widetilde{\sigma}_{zzr}}{\mathrm{d}z} = -\sum_{k=2}^{N-1} X_{rk}^{(1)}\widetilde{\sigma}_{xzk} + q\widetilde{\sigma}_{yzr} - \frac{1}{a_2}\sum_{k=2}^{N-1} f_{rk}\widetilde{u}_{zk},$$

$$\begin{aligned}\frac{\mathrm{d}\widetilde{\sigma}_{xzr}}{\mathrm{d}z} = {} & -a_1\sum_{k=2}^{N-1} X_{rk}^{(2)}\widetilde{u}_{xk} - \frac{a_4^2}{a_5}\sum_{k=2}^{N-1} f_{rk}\widetilde{u}_{xk} + a_6q^2\widetilde{u}_{xr} + (a_3+a_6)q\sum_{k=2}^{N-1} X_{rk}^{(1)}\widetilde{u}_{yk} - b_1\sum_{k=2}^{N-1} X_{rk}^{(2)}\widetilde{w}_{xk} \\ & - b_1q^2\widetilde{w}_{xr} + 2b_1q\sum_{k=2}^{N-1} X_{rk}^{(1)}\widetilde{w}_{yk} + a_4\sum_{k=2}^{N-1} X_{rk}^{(1)}\widetilde{\sigma}_{zzk},\end{aligned}$$

$$\begin{aligned}
\frac{\mathrm{d}\widetilde{\sigma}_{yzr}}{\mathrm{d}z} =& -(a_3+a_6)q\sum_{k=2}^{N-1}X_{rk}^{(1)}\widetilde{u}_{xk}-a_6\sum_{k=2}^{N-1}X_{rk}^{(2)}\widetilde{u}_{yk}+a_1q^2\widetilde{u}_{yr}\\
&+2b_1q\sum_{k=2}^{N-1}X_{rk}^{(1)}\widetilde{w}_{xk}-b_1\sum_{k=2}^{N-1}X_{rk}^{(2)}\widetilde{w}_{yk}-b_1q^2\widetilde{w}_{yr}+a_4q\widetilde{\sigma}_{zzr},\\
\frac{\mathrm{d}\widetilde{H}_{xzr}}{\mathrm{d}z} =& -b_1\sum_{k=2}^{N-1}X_{rk}^{(2)}\widetilde{u}_{xk}-b_1q^2\widetilde{u}_{xr}-2b_1q\sum_{k=2}^{N-1}X_{rk}^{(1)}\widetilde{u}_{yk}-b_2\sum_{k=2}^{N-1}X_{rk}^{(2)}\widetilde{w}_{xk}+b_2q^2\widetilde{w}_{xr},\\
\frac{\mathrm{d}\widetilde{H}_{yzr}}{\mathrm{d}z} =& -2b_1q\sum_{k=2}^{N-1}X_{rk}^{(1)}\widetilde{u}_{xk}-b_1\sum_{k=2}^{N-1}X_{rk}^{(2)}\widetilde{u}_{yk}-b_1q^2\widetilde{u}_{yr}-b_2\sum_{k=2}^{N-1}X_{rk}^{(2)}\widetilde{w}_{yk}+b_2q^2\widetilde{w}_{yr},\\
\frac{\mathrm{d}\widetilde{u}_{zr}}{\mathrm{d}z} =& a_4\sum_{k=2}^{N-1}X_{rk}^{(1)}\widetilde{u}_{xk}-a_4q\widetilde{u}_{yr}+a_5\widetilde{\sigma}_{zzr},
\end{aligned}$$

where $2\leqslant r\leqslant N-1$.

The state equations for CSSS are

$$\begin{aligned}
\frac{\mathrm{d}\widetilde{u}_{xr}}{\mathrm{d}z} =& a_2\widetilde{\sigma}_{xzr}-\sum_{k=2}^{N-1}X_{rk}^{(1)}\widetilde{u}_{zk}\quad(2\leqslant r\leqslant N),\quad \frac{\mathrm{d}\widetilde{u}_{yr}}{\mathrm{d}z}=a_2\widetilde{\sigma}_{yzr}-q\widetilde{u}_{zr}\quad(2\leqslant r\leqslant N-1),\\
\frac{\mathrm{d}\widetilde{w}_{xr}}{\mathrm{d}z} =& b_3\widetilde{H}_{xzr}\quad(2\leqslant r\leqslant N),\quad \frac{\mathrm{d}\widetilde{w}_{yr}}{\mathrm{d}z}=b_3\widetilde{H}_{yzr}\quad(2\leqslant r\leqslant N-1),\\
\frac{\mathrm{d}\widetilde{\sigma}_{zzr}}{\mathrm{d}z} =& -\sum_{k=2}^{N}X_{rk}^{(1)}\widetilde{\sigma}_{xzk}+q\widetilde{\sigma}_{yzr}-\frac{1}{a_2}\sum_{k=2}^{N-1}f_{1rk}\widetilde{u}_{zk}\quad(2\leqslant r\leqslant N-1),\\
\frac{\mathrm{d}\widetilde{\sigma}_{xzr}}{\mathrm{d}z} =& -a_1\sum_{k=2}^{N}X_{rk}^{(2)}\widetilde{u}_{xk}-\frac{a_4^2}{a_5}\sum_{k=2}^{N}f_{1rk}\widetilde{u}_{xk}+a_6q^2\widetilde{u}_{xr}+a_1\sum_{k=2}^{N}f_{Nrk}\widetilde{u}_{xk}+(a_3+a_6)q\sum_{k=2}^{N-1}X_{rk}^{(1)}\widetilde{u}_{yk}\\
&-b_1\sum_{k=2}^{N-1}X_{rk}^{(2)}\widetilde{w}_{xk}-b_1q^2\widetilde{w}_{xr}+b_1\sum_{k=2}^{N}f_{Nrk}\widetilde{w}_{xk}+2b_1q\sum_{k=2}^{N}X_{rk}^{(1)}\widetilde{w}_{yk}\\
&+a_4\sum_{k=2}^{N-1}X_{rk}^{(1)}\widetilde{\sigma}_{zzk}\quad(2\leqslant r\leqslant N),\\
\frac{\mathrm{d}\widetilde{\sigma}_{yzr}}{\mathrm{d}z} =& -(a_3+a_6)q\sum_{k=2}^{N}X_{rk}^{(1)}\widetilde{u}_{xk}-a_6\sum_{k=2}^{N-1}X_{rk}^{(2)}\widetilde{u}_{yk}+a_1q^2\widetilde{u}_{yr}\\
&+2b_1q\sum_{k=2}^{N}X_{rk}^{(1)}\widetilde{w}_{xk}-b_1\sum_{k=2}^{N-1}X_{rk}^{(2)}\widetilde{w}_{yk}-b_1q^2\widetilde{w}_{yr}+a_4q\widetilde{\sigma}_{zzr}\quad(2\leqslant r\leqslant N-1),\\
\frac{\mathrm{d}\widetilde{H}_{xzr}}{\mathrm{d}z} =& -b_1\sum_{k=2}^{N}X_{rk}^{(2)}\widetilde{u}_{xk}-b_1q^2\widetilde{u}_{xr}-2b_1q\sum_{k=2}^{N-1}X_{rk}^{(1)}\widetilde{u}_{yk}-b_2\sum_{k=2}^{N}X_{rk}^{(2)}\widetilde{w}_{xk}+b_2q^2\widetilde{w}_{xr}\quad(2\leqslant r\leqslant N),\\
\frac{\mathrm{d}\widetilde{H}_{yzr}}{\mathrm{d}z} =& -2b_1q\sum_{k=2}^{N}X_{rk}^{(1)}\widetilde{u}_{xk}-b_1\sum_{k=2}^{N-1}X_{rk}^{(2)}\widetilde{u}_{yk}-b_1q^2\widetilde{u}_{yr}\\
&-b_2\sum_{k=2}^{N-1}X_{rk}^{(2)}\widetilde{w}_{yk}+b_2q^2\widetilde{w}_{yr}\quad(2\leqslant r\leqslant N-1),\\
\frac{\mathrm{d}\widetilde{u}_{zr}}{\mathrm{d}z} =& a_4\sum_{k=2}^{N}X_{rk}^{(1)}\widetilde{u}_{xk}-a_4q\widetilde{u}_{yr}+a_5\widetilde{\sigma}_{zzr}\quad(2\leqslant r\leqslant N-1)
\end{aligned}$$

with $f_{1rk}=X_{r1}^{(1)}X_{1k}^{(1)}$, $f_{Nrk}=X_{rN}^{(1)}X_{Nr}^{(1)}$, and $f_{rk}=f_{1rk}+f_{Nrk}$.